The Effects of a Ternary Electrolyte Additive System on the Electrode/Electrolyte Interfaces in High Voltage Li-Ion Cells

Lénaïc Madec,[a] Lin Ma,[b] Kathlyne J. Nelson,[a,*] Remi Petibon,[b] Jon-Paul Sun,[a] Ian G. Hill,[a] and Jeff R. Dahn[a,b,**,z]

[a]*Department of Physics and Atmospheric Science, Dalhousie University, Halifax, B3H4R2, Canada*
[b]*Department of Chemistry, Dalhousie University, Halifax, B3H4R2, Canada*

The effects of a ternary electrolyte additive system on $Li[Ni_{0.42}Mn_{0.42}Co_{0.16}]O_2$ (NMC442)/graphite pouch cells balanced for 4.7 V was thoroughly investigated. The additive system consisted of 2% prop-1-ene-1,3-sultone (PES) + 1% methylene methane disulfonate + 1% tris-(trimethylsilyl)-phosphite (TTSPi) which is denoted "PES211". "PES211" significantly improved the capacity retention, impedance and gas evolution of NMC442/graphite pouch cells cycled at constant current up to 4.4 V or 4.5 V. X-ray photoelectron spectroscopy results suggest more stable and passivating SEI films at both graphite and NMC442 surfaces due to the preferential electrochemical reaction of PES and MMDS as well as the preferential chemical reaction of TTSPi at the graphite surface. "PES211" modifies the reactivity of LiPF$_6$ salt at the graphite surface and hinders its degradation at high potential. However, during extended exposure to 4.5 V, less passivating SEI films were observed leading to extensive electrolyte degradation, capacity loss, impedance increase and gas evolution even for NMC442/graphite pouch cells containing "PES211".

High volumetric energy density lithium ion (Li-ion) cells can be made if positive electrode materials like $Li[Ni_{0.4}Mn_{0.4}Co_{0.2}]O_2$ (NMC442) can be operated to 4.7 V. However, severe electrolyte degradation occurs at the positive electrode surface when such materials are charged above 4.3 V vs. Li/Li$^+$ which lead to large cell impedance and short lifetime.[1,2] To overcome this limitation, the use of electrolyte additives is one of the most simple, economical and effective approaches.[3,4] Electrolyte additives are known to hinder unwanted parasitic reactions of electrolyte solvents and/or salts that occur during cycling/storage at the electrolyte/electrode interfaces by modifying the Solid Electrolyte Interphase (SEI).[5]

Vinylene carbonate (VC)[6] is perhaps the most famous and widely used additive as it has been shown to greatly improve cycle/calendar life and thermal stability of different Li-ion systems.[7–13] However, the charge-discharge capacity loss, impedance and gas evolution of cells containing VC all increase at high potentials[14] and high temperatures[15] due to extensive electrolyte degradation. To overcome these limitations and enable the use of high voltage Li-ion cells, sulfur-containing additives have been recently proposed by different research groups.[16–20]

Prop-1-ene-1,3-sultone (PES, Figure 1) was first proposed as a SEI film forming additive by Li et al.[21,22] in LiCoO$_2$/graphite cells using PC-based electrolyte. Later, they showed that using PES in ethylene carbonate (EC):ethyl methyl carbonate (EMC) (1:2 by weight) electrolyte also greatly improved the capacity retention of $LiNi_{0.5}Mn_{1.5}O_4$/Li half cells compared to control cells[23] and in LiMn$_2$O$_4$/graphite cells tested at 60°C compared to cells using VC.[24] For this later case, PES was also found to lower the gas production by a factor of 3 after 150 cycles at 60°C compared to the use of VC. Li et al. attributed the beneficial effects of PES to its preferential reaction and the formation of more protective and stable SEI films at both electrode surfaces. Xia et al.[25] and Nelson et al.[26] also demonstrated the superiority of PES over VC as an electrolyte additive for 1 M LiPF$_6$ in EC:EMC (3:7 by weight) in $Li[Ni_{1/3}Mn_{1/3}Co_{1/3}]O_2$ (NMC)/graphite pouch cells balanced for 4.2 V. They showed that the use of 2% PES nearly eliminated gas production during storage at 4.2 V and 60°C whereas VC did not. More recently, using XPS experiments, Madec et al.[27] showed that in NMC/graphite pouch cells balanced for 4.2 V, PES forms more protective and stable SEI films at both graphite and NMC surfaces which might explain the improved electrochemical

performance as well as the lower production of gas observed with PES compared to control electrolyte. They attributed these results to the preferential reaction of PES at both graphite and NMC surfaces that led to an additional contribution of sulfite species and substantially less LiF compared to control electrolyte.

Methylene methane disulfonate (MMDS, Figure 1) has also been recently proposed as an efficient sulfur-containing additive for high voltage Li-ion cells. Zuo et al.[28] showed that MMDS dramatically improved the capacity retention of LiCoO$_2$/graphite cells with 1 M LiPF$_6$ in EC:EMC (1:2 by weight) at 4.5 V. Zuo et al.[29] also showed a significant improvement of the capacity retention of $LiNi_{0.5}Co_{0.2}Mn_{0.3}O_2$/graphite cells using MMDS in 1 M LiPF$_6$ in EC:EMC (1:2 by weight) but only when cycled at 4.4 V, while they observed little difference at 4.2 V compared to cells without MMDS. In both studies, they ascribed the enhanced cycling performance of the cells to the modification of the positive electrode SEI films by MMDS which hindered solvent decomposition and led to lower impedance compared to control cells. Later, MMDS was shown to improve the capacity retention of LiMn$_2$O$_4$ electrodes cycled at elevated temperature in 1 M LiPF$_6$ in EC:EMC:dimethyl carbonate (DMC) (1:1:1 by weight)[30–32] due to reduction of both the decomposition of the electrolyte and the dissolution of Mn ions in the electrolyte. Xia et al.[16,18] also studied the use of MMDS in NMC/graphite pouch cells with 1 M LiPF$_6$ in EC:EMC (3:7 by weight) at 4.2 V. They showed that MMDS reduced the rate of parasitic reactions (i.e. MMDS increased the coulombic efficiency and lowered the charge end point capacity slippage), decreased the impedance measured after storage and after cycling and reduced the amount of gas produced during formation compared to cells without MMDS.

Silyl substituted electrolyte additives such as tris-(trimethylsilyl)-phosphite (TTSPi, Figure 1) were recently developed by Wildcat Discovery Technologies (California, USA) to improve the cycling performance of various positive electrode materials at high voltage and/or elevated temperature.[33] Sinha et al.[34] studied the effect of TTSPi in NMC/graphite pouch cells with 1 M LiPF$_6$ in EC:EMC (3:7 by weight) at 4.2 V and showed that TTSPi not only increased the coulombic efficiency but also reduced the cell impedance significantly. Mai et al.[35] also showed that adding only 0.5 wt% of TTSPi in 1 M LiPF$_6$ EC:DMC (1:2 by volume) significantly improved the impedance and capacity retention of NMC/Li half cells at 4.5 V which they ascribed to a preferential oxidation of TTSPi that formed a protective SEI on the NMC. Song et al.[36] also used TTSPi as a multifunctional additive to improve the electrochemical performance of $LiNi_{0.5}Mn_{1.5}O_4$ at 5 V. They showed that TTSPi hindered the decomposition of LiPF$_6$ by hydrolysis, scavenged HF and therefore limited Mn/Ni dissolution and
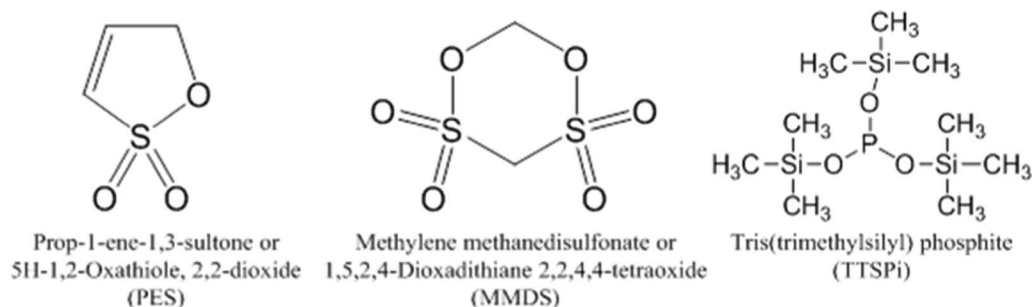
Figure 1. Molecular formula and structural information for prop-1-ene-1,3-sultone (PES), methylene methanedisulfonate (MMDS) and tris-(trimethylsilyl)-phosphite (TTSPi).

formed a protective positive electrode SEI to limit electrolyte decomposition at high voltages. Similarly, Yim et al.[37] used TTSPi to improve the cycling stability of 0.5 Li$_2$MnO$_3$ • 0.5 Li(Ni$_{0.4}$Mn$_{0.4}$Co$_{0.2}$)O$_2$ positive electrode material. They proposed that the trivalent phosphorus in TTSPi can scavenge oxygen gas in the cell, that the electrophilic phosphorus and silicon can remove nucleophilic lithium oxide species by a chemical scavenging reaction and that the silyl ether component can prevent transition metal dissolution through a fluoride scavenging reaction.

Recently, Ma et al.[38] showed that the combination of the three additives PES, MMDS and TTSPi (2:1:1 wt%, referred to as "PES211") stabilized the impedance and improved the capacity retention of NMC442/graphite pouch cells cycled at constant current up to 4.4 V or to 4.5 V and also increased the safety of the cells.[39] Later, Nelson et al.[40] showed that NMC442/graphite pouch cells cycled aggressively at 40°C with a 20 h hold at the top of every charge displayed a dramatic capacity loss and large impedance increase which was mitigated to some extent by the use of "PES211". Here, the effects of the ternary additive system, "PES211", on the electrode/electrolyte interphases was investigated by correlating the electrochemical performance of NMC442/graphite pouch cells with thorough X-ray photoelectron spectroscopy (XPS) analysis of the SEI films formed at the surfaces of both graphite and NMC442 electrodes during formation and after different cycling protocols.

Experimental

Cell preparation.—1 M LiPF$_6$ (BASF, purity 99.94, water content < 20 ppm) in EC:EMC (3:7 by weight, BASF, water content < 20 ppm) was used as the control electrolyte. To this electrolyte, either 2 wt% vinylene carbonate (VC from BASF, 99.97%), 2 wt% PES (Lianchuang Medicinal Chemistry Co., 98.2%) or 1 wt% MMDS (Tinci Materials Technology, 98.7%) or 1 wt% TTSPi (Sigma-Aldrich, > 95%) were added as single additives. The combination of 2% PES + 1% MMD + 1% TTSPi (by weight, referred to as "PES211") was also used as ternary additive system. Machine-made 240 mAh LiNi$_{0.42}$Mn$_{0.42}$Co$_{0.16}$O$_2$ (NMC442)/graphite pouch cells balanced for 4.7 V operation were obtained dry (vacuum sealed with no electrolyte) from Li-Fun Technology (Xinma Industry Zone, Golden Dragon Road, Tianyuan District, Zhuzhou City, Hunan Province, PRC, 412000). The pouch cells are 40 mm long × 20 mm wide × 3.5 mm thick. The electrode composition in the cells was as follows in wt%: Positive electrode - 96.2%:1.8%:2.0% = Active Material:Carbon Black:PVDF Binder; Negative electrode - 95.4%:1.3%:1.1%:2.2% = Active material:Carbon Black:CMC:SBR. The positive electrode had a total thickness of 105 μm and was calendared to an active material density of 3.55 g/cm^3. The negative electrode coating had a total thickness of 110 μm and was calendared to an active material density of 1.55 g/cm^3. The positive electrode coating had an areal density of 16 mg/cm^2 (single side) and the negative electrode had an areal density of 9.5 mg/cm^2 (single side). The positive electrode dimensions were 200 mm × 26 mm and the negative electrode dimensions were 204 mm × 28 mm. Both electrodes were

coated on both sides, except for small regions on one side at the end of the foils leading to an active area of approximately 100 cm^2. The electrodes are spirally wound, not stacked, in these pouch cells. After heating to 80°C under vacuum for 12 h to remove residual water, the pouch cells were filled with 0.9 g of electrolyte in an argon-filled glove box then vacuum-sealed at -94 kPa (relative to atmospheric pressure) using a compact vacuum sealer (MSK-115A, MTI Corp.). For each of the following electrochemical experiments, two identical pouch cells were prepared for reproducibility.

Cell formation and cycling protocols.—After filling, formation was performed using a Maccor 4000 series cycler. Cells were placed in a home-made temperature-controlled box at 40. ± 0.1°C and held at 1.5 V for 24 h (for completion of wetting) then charged to 3.8 V at 12 mA (C/20). Cells were then cut open in an argon-filled glove box to release any gas generated and vacuum sealed again. Cells were then charged either to 4.4 V or 4.5 V at 12 mA (C/20) and the degassing procedure was repeated. For the XPS study, some selected cells were further charged to 4.7 V at 12 mA (C/20). Then, cells were discharged to 2.8 V at 12 mA (C/20). For all pouch cells dedicated to the XPS study, at each charge/discharge step during the formation process, the potential was held until the measured current decreased to 0.005C so that electrodes were in electrochemical equilibrium.

Constant current cycling (CC) for XPS.—Cells were cycled using a Maccor 4000 series battery cycler between 4.4 or 4.5 V and 2.8 V at 40. ± 0.1°C and 12 mA (C/20) for 24 cycles and stopped either fully charged at 4.4 or 4.5 V or fully discharged at 2.8 V.

Constant current-constant voltage cycling (CC-CV) for XPS.—Cells were cycled using a Maccor 4000 series battery cycler at 40. ± 0.1°C. One cycle of charge-hold-discharge protocol consisted of a constant current charge to 4.4 or 4.5 V at 48 mA (C/5) followed by a constant voltage step at the top of charge (4.4 or 4.5 V) for 24 h, then a constant current discharge to 2.8 V at 48 mA (C/5).

CC and CC-CV procedures coupled with impedance measurements.—Additional cells were subjected to either CC or CC-CV cycling while their impedance spectra measured every 12 cycles or 4 cycles, respectively. A system built in house[41] consisting of a Neware Battery Testing System connected to a computer equipped with a Gamry frequency response analyzer (FRA) card was used for these experiments. During impedance measurements, relays disconnected the cells from the Neware cycler and connected them to the FRA card to have their impedance spectra measured. To accommodate the impedance measurement, the CC-CV protocol described above was slightly altered. Every 12 (CC) or 4 (CC-CV) cycles, cells underwent a slow C/20 constant current cycle while impedance spectra were measured every 0.1 V from 3.6 V to the top of charge (4.4 or 4.5 V) during both charge and discharge.

Gas measurements.—Gas evolution measurements employing
Archimedes' principle were performed before and after each for-
mation step and after the constant current (CC) or the charge-hold-
discharge (CC-CV) cycling by weighing cells submerged in de-
ionized nanopure water (18 M) at 20 ± 1°C. This procedure is fully
described in reference 42.

X-ray Photoelectron Spectroscopy (XPS).—*Sample
preparation.*—After formation, CC and CC-CV cycling, pouch
cells were disassembled in an argon-filled glove box within the first
12 h following the end of the electrochemical process. Graphite
and NMC442 electrodes were cut from the pouch cell electrodes
with a precision punch and washed twice by immersion into 0.8 mL
of EMC solvent (BASF) in a clean and dry glass vial with a mild
manual agitation for 10 s to remove the majority of the LiPF$_6$ salt.
Air sensitive samples were then mounted onto a molybdenum holder
using a copper conductive tape (3M) under argon and placed into a
special transfer system.[20] The latter was then put under vacuum at
approx. 10^{-3} mbar for 1 h and then connected to the spectrometer
where samples were loaded under a pressure of $\sim10^{-3}$ mbar. All
samples were kept at 10^{-8} mbar for one night before analysis to
ensure a strictly identical vacuum procedure.

Data acquisition and treatment.—XPS was performed on a SPECS
spectrometer equipped with a Phoibos 150 hemispherical energy an-
alyzer and using Mg Kα radiation ($h\nu$ = 1253.6 eV). The analyzed
sample area was $\sim2 \times 3$ mm^2 which gave results representative of
the whole electrode. Core spectra were recorded in the fixed analyzer
transmission (FAT) mode with a 20 eV pass energy at an operating
pressure $<2 \times 10^{-9}$ mbar. Short acquisition time spectra were first
recorded as a reference to follow any possible sample degradation
during the analysis. Data treatment was performed using CasaXPS
software. The binding energy scale was calibrated from the C1s peak
at 285 eV (C-C/C-H) and the O1s peak at 529.6 eV (O^{2-} anion from
the NMC442) for the graphite and NMC422 electrodes, respectively.
A nonlinear Shirley-type background[43] was used for core peaks anal-
ysis while 70% Gaussian - 30% Lorentzian Voigt peak shapes and
full width at half-maximum (fwhm) constraint ranges were selected
to optimize areas and peak positions.

Results and Discussion

Long term cycling and impedance.—Figure 2 shows the discharge
capacity and the total resistance, R$_{total}$, (measured at 4.4 V), as function
of cycle number for the NMC442/graphite pouch cells that underwent
either the CC or the charge-hold-discharge (CC-CV) cycling cou-
pled with impedance measurements. Here, R$_{total}$ is the diameter of
the "semicircle" or overlapping semicircles of the Nyquist plot and
represents the sum of the charge transfer resistance, the resistance as-
sociated with the motion of the Li ion through the SEI and any current
collector/electrode resistance for both electrodes. Results from cells
with 2 wt% VC are also shown for comparison as VC is well known
to improve the capacity retention of Li-ion cells. Note that control
cells (no additive) are not presented here but showed very poor ca-
pacity retention with $\sim70\%$ (~160 mAh) of the initial capacity after
only 20 cycles (see Figure 5b). Compared to control cells, the use
of 2% VC may appear useful up to 20 cycles, however, beyond that
point, 2% VC cells showed dramatic capacity fade due to resistive (see
R$_{total}$, Figure 2b) and unstable SEI layers.[14] During CC cycling at only
4.4 V, the use of 2% PES outperformed 2% VC electrolyte which
shows the benefit of using PES rather than VC for cells destined for
high potential. When the upper cutoff potential was increased to 4.5 V,
however, cells with 2% PES immediately showed a lower capacity re-
tention followed by a severe capacity fade after 115 cycles. These
phenomena were associated to an increase of the impedance as soon
as the voltage range was increased to 4.5 V indicating an increase of
the parasitic reactions and the formation of resistive SEI films upon
exposure to potentials above 4.4 V. Cells with "PES211" had the best
capacity retention (about 87% after 285 cycles) during constant cur-
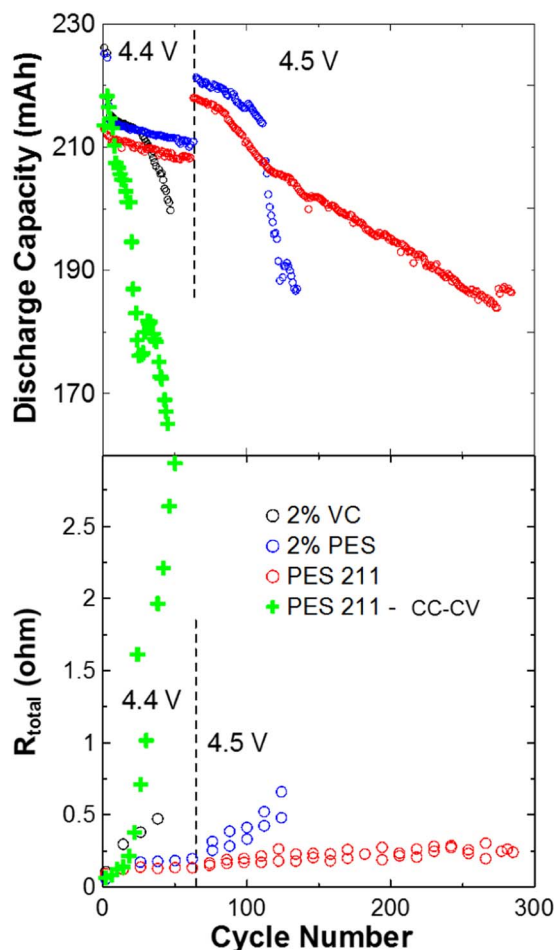

Figure 2. a) Discharge capacity as a function of cycle number for
NMC442/graphite pouch cells undergoing CC cycling between 2.8 and 4.4 V
then 4.5 V at C/5 (48 mA) and 40. ± 0.1°C for selected electrolyte blends. The
dotted line indicates when the upper cutoff voltage was increased from 4.4 V
to 4.5 V. For PES 211 electrolyte, data for cells undergoing the charge-hold-
discharge (CC-CV) procedure between 2.8 and 4.4 V (48 mA, C/5 – 20 h, see
Experimental section) at 40. ± 0.1°C are also presented for comparison. b)
Combination of the charge transfer resistance and the resistance due to motion
of ions through the SEI layers for the full cell, Rtotal, measured at 4.4 V as a
function of cycle number for the same cells.

rent cycling to 4.5 V which suggests more stable SEI films with low
impedance as shown in Figure 2b. Cells with "PES211" were also
subjected to the charge-hold-discharge (CC-CV) protocol to an upper
cutoff potential of 4.4 V. Figure 2 shows that those cells failed rapidly
due to extensive impedance increase. Figure 2 demonstrates that the
CC-CV protocol is much more challenging than the CC protocol. This
is a good lesson for researchers who may promote CC cycling results
as indicative of commercially relevant results.

***dQ/dV vs. V measured during the initial stages of the formation
cycle.***—Figure 3b shows the differential capacity (dQ/dV) versus V
curves of the NMC442/graphite pouch cells between 1.6 and 3.5 V
during the formation cycle. The voltage versus capacity during the
first 14 mAh of the formation cycle is also showed (Figure 3a) so
that readers can have a better understanding of the dQ/dV versus V
curves. Control cells showed a pronounced peak at 2.9 V (graphite at
~0.8 V vs. Li/Li$^+$) due to the reduction of EC at the graphite
surface.[44,45] When 1% TTSPi was added, the reduction peak of
EC was unaffected and no additional peak was detected indicating
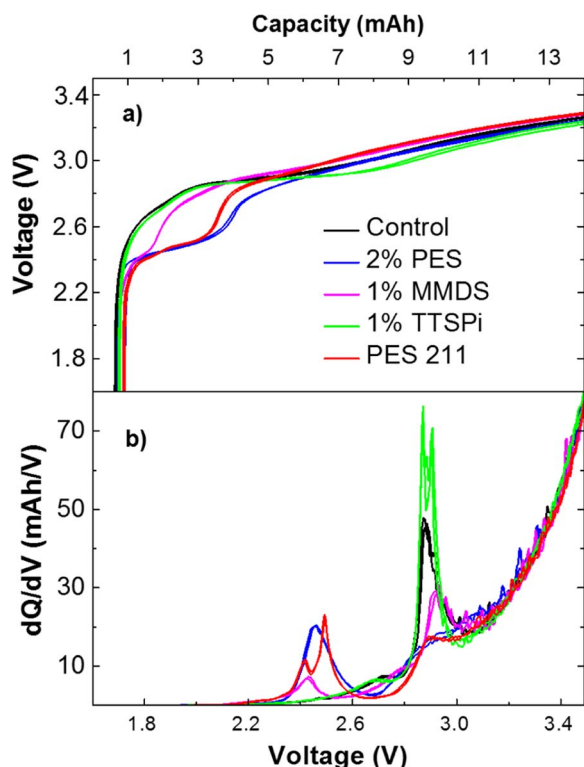that TTSPi may not undergo an electrochemical reduction during

Figure 3. a) Voltage versus capacity during the first 14 mAh of the formation cycle and b) differential capacity (dQ/dV) versus potential (V) during the early stages of the formation cycle of NMC442/graphite pouch cells at C/20 and 40. ± 0.1°C for the different electrolyte blends studied here.

formation as expected from previous studies.[34,36] To validate this hypothesis, the consumption/reaction of TTSPi was probed using liquid electrolyte analysis by gas chromatography/mass spectroscopy (GC-MS), following the procedure described by Petibon et al.[46,47] The total consumption of TTSPi was found after formation at 3.5 V and more interestingly TTSPi was also totally consumed when a cell was simply filled with 1% TTSPi electrolyte and put in a freezer for 24 h without any charging at all (Figure S1). This result suggests that TTSPi reacts chemically in NMC442/graphite pouch cell. Figure 3 shows that the use of 1% MMDS partially decreased the EC reduction at 2.9 V due to the preferential reduction of MMDS at 2.4 V (graphite at ~1.35 V vs. Li/Li⁺).[16] For 2% PES electrolyte, the EC reduction was almost supressed due to the preferential reduction of PES at 2.45 V (graphite at ~1.35 V vs. Li/Li⁺).[25] Finally, when "PES211" was used, the EC reduction was nearly eliminated due to the combined reduction of both MMDS and PES at 2.4 V and 2.5 V, respectively.

Gas analysis.—Figure 4 shows the volume of gas evolved in the NMC442/graphite pouch cells at 40°C during (a) formation and (b) during the CC and charge-hold-discharge (CC-CV) cycling at 4.4 and 4.5 V. The data in Figure 4 is for the cells used for the XPS studies. For reference, the initial volumes of the pouch cells is 2.2 mL. During the formation process (Figure 4a), control cells produced about 0.8 mL of gas while the use of 1% MMDS slightly the gas production to 0.6 mL. For 1% TTSPi and 2% PES electrolytes, however, the gas generated during formation decreased to 0.35 mL and 0.15 mL, respectively. TTSPi and especially PES are therefore very efficient gas reducing agents during formation. When "PES211" electrolyte was used, an intermediate volume of gas was formed (0.25 mL) indicating a combined effect of the additives. Figure 4b shows that the use of "PES211" greatly decreased the volume of gas produced during cycling compared to control cells. However, for the charge-hold-discharge (CC-CV) cycling at 4.4 V, the volume of gas generated with "PES211" increased and further increased when CC-CV cycling was
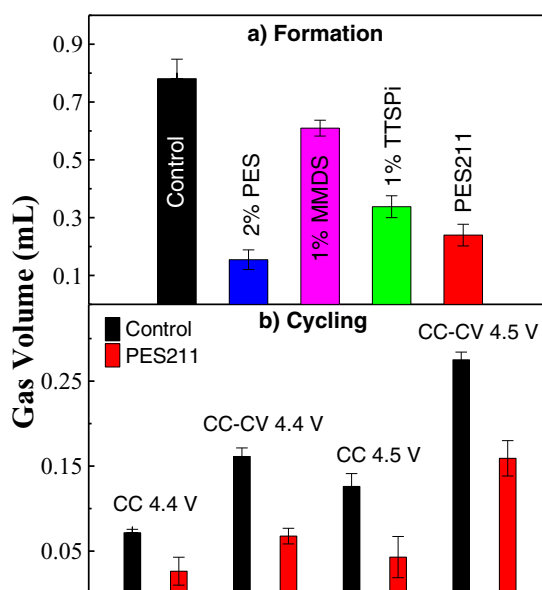

Figure 4. Volume of gas evolved in NMC442/graphite pouch cells for the different electrolytes a) during the formation process at C/20 (12 mA) and 40. ± 0.1°C and b) during the CC and charge-hold-discharge (CC-CV) cycling (see Experimental section) at 40. ± 0.1°C.

used to 4.5 V suggesting that extensive electrolyte degradation occurs as soon as the cells are exposed for too much time at potentials above 4.4 V.

Figure 5 shows the discharge capacity for the short term CC and charge-hold-discharge (CC-CV) cycling between 2.8 and 4.4 or
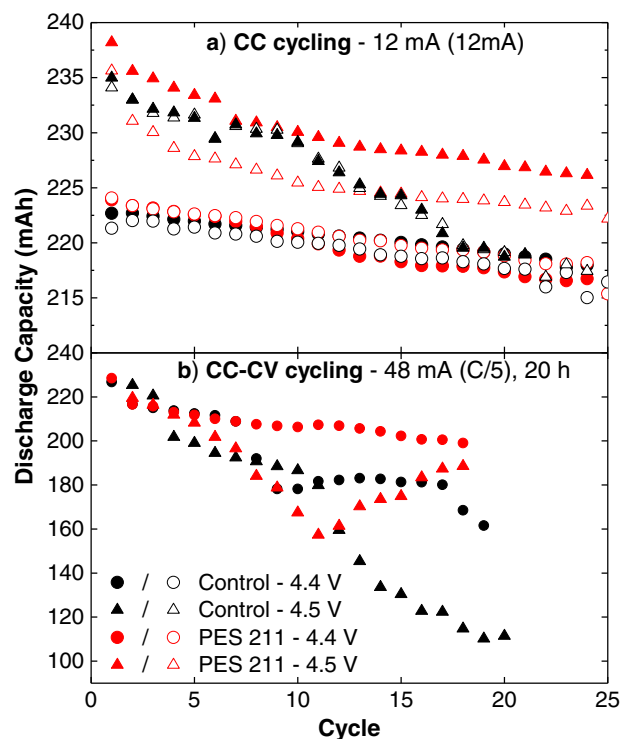

Figure 5. Discharge capacity as function of cycle number for NMC442/graphite pouch cells with control and "PES211" electrolytes undergoing a) the 12 mA (C/20) CC cycling and b) the charge-hold-discharge (48 mA (C/5) CC- 20 h CV) cycling between 2.8-4.4 V and 2.8-4.5 V at 40. ± 0.1°C.
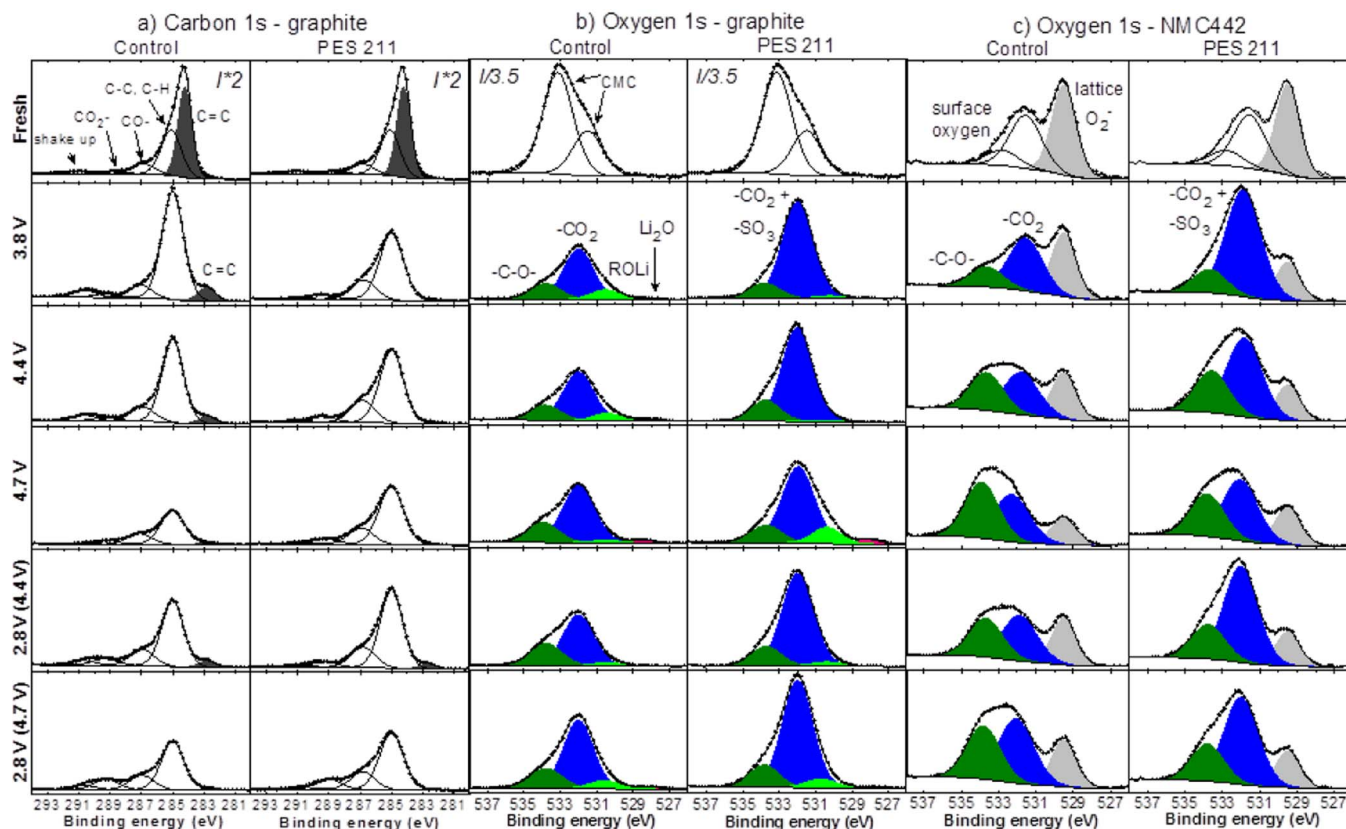
Figure 6. Carbon 1s (a) and Oxygen 1s (b) XPS core spectra of graphite electrodes as well as Oxygen 1s XPS core spectra of NMC422 electrodes (c) for control and "PES211" electrolytes, as taken from NMC442/graphite pouch cells during formation at 3.8 V, 4.4 V and 4.7 V during charge and at 2.8 V during the discharge following the charges to 4.4 V and 4.7 V.

4.5 V at C/20 and 40. ± 0.1°C for the NMC442/graphite pouch cells with control and "PES211" electrolytes. Cells with control electrolyte showed good capacity retention during the 25 cycles tested for CC cycling at 4.4 V and poor capacity retention at 4.5 V while cells with "PES211" showed good capacity retention for both upper cutoff potentials in CC cycling. The cells tested in charge-hold-discharge (CC-CV) as shown in Figure 5b experienced a failure of the 40°C temperature box, where the temperature cooled to 23°C for a few cycles in the middle of the testing, before it was repaired. This is why there is anomalous behavior for some of the cells in Figure 5b. Nevertheless, control cells tested with charge-hold-discharge cycling showed extensive capacity loss when tested at 4.5 V while "PES211" cells did not, once their temperature restabilized at 40°C. The y-axis scales in Figures 5a and 5b differ significantly showing, again, that charge-hold-discharge (CC-CV) testing is much more severe that CC testing in agreement with Figure 2.

XPS analysis.—To investigated effects of the ternary additive system "PES211" on the electrode/electrolyte interfaces by XPS, SEI films on both graphite and NMC442 surfaces for control, 2% PES, 1% MMDS, 1% TTSPi and "PES211" electrolytes were analyzed at various stages of the formation cycle, at 3.8 V, 4.4 V, 4.5 V and 4.7 V during charge and at 2.8 V after discharge following charge at 4.4 V, 4.5 V and 4.7 V. A separate pouch cell was used for each measurement. For control and "PES211" electrolytes, SEI films were also analyzed after the 25 cycles of CC and charge-hold-discharge (CC-CV) cycling shown in Figure 5 both at top of charge and bottom of discharge. However, for clarity and brevity, only selected XPS spectra will be presented here. In the different Figures presented below, the core level spectra for a given element were normalized to show the relative intensities/amount of the given element between samples.

Formation of the cells.—Figure 6 shows the Carbon 1s (a) and Oxygen 1s (b) XPS core spectra of graphite electrodes as well as Oxygen 1s XPS core spectra of NMC422 electrodes (c) for control electrolyte and "PES211" electrolyte as taken from NMC442/graphite pouch cells during formation at 3.8 V, 4.4 V and 4.7 V during charge and 2.8 V during the discharge following the charge at 4.4 V and 4.7 V. The C 1s core spectrum of the fresh graphite electrode showed five components at 284.1, 285.0, 286.9, 288.6 and 290.8 eV attributed to the C=C bonds from the graphite, C-C/C-H from the SBR binder, C=O and COOR carbons as well as the "shake up" satellite from the graphite, respectively.[48,49] During formation to 3.8 V then to higher potentials, the intensity of the graphite peak at ~282.7 eV significantly decreased for control electrolyte indicating the continuous formation of a SEI film on the graphite surface. For "PES211" electrolytes, however, the graphite peak was barely visible even at 3.8 V which indicates the rapid formation of a relatively thick SEI film compared to control electrolyte possibly due to the preferential reduction of both PES and MMDS at the graphite surface (Figure 3). This suggestion is supported by a similar evolution of the graphite peak during formation for 2% PES and 1% MMDS electrolytes compared to "PES211" cells while the graphite peak evolution for 1% TTSPi electrolyte was close to control cells (Figure S2 in the supporting information). Figure 6a also shows that when formed at 4.7 V, the carbon content of the SEI on the graphite electrode decreased significantly for control electrolyte indicating a large change of the composition of the SEI most likely due products of electrolyte oxidation at the positive electrode migrating to the negative. When "PES211" was used, however, almost no change of carbon content was observed at 4.7 V most likely due to a more stable SEI film at the positive electrode, limiting oxidation products. After discharge, no significant change of the graphite peak intensity and carbon content was observed for both control and "PES211" electrolytes.
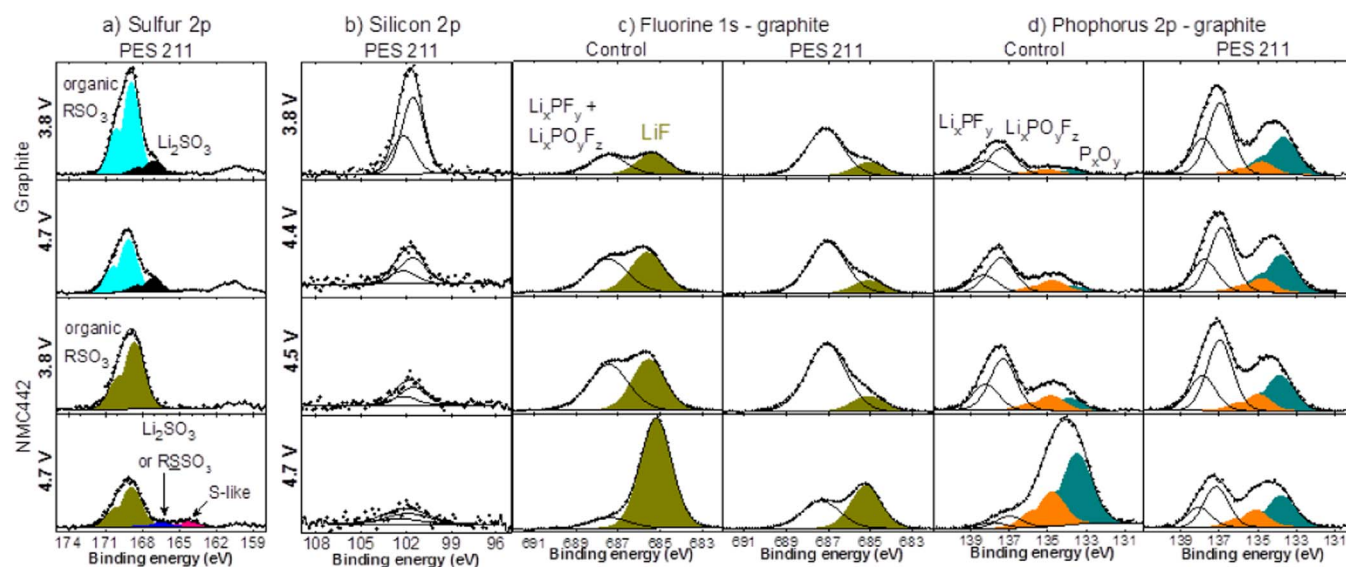
Figure 7. Sulfur 2p (a) XPS core spectra of graphite and NMC442 electrodes during formation at 3.8 V and 4.7 V as well as silicon 2p (b), fluorine 1s (c) and phosphorus 2p (d) XPS core spectra of graphite electrodes during formation at 3.8 V, 4.4 V, 4.5 V, 4.7 V, as taken from NMC442/graphite pouch cells for control and/or "PES211" electrolytes.

In the O 1s spectra of the graphite electrodes (Figure 6b), the two components of the fresh electrode were replaced by two new main components at 532 and 533.8 eV due to the simultaneous covering of the graphite and CMC binder by the SEI.[50] The peak at 533.8 eV is assigned to -C-O- bonds from $ROCO_2Li$ and/or ether derivatives.[51,52] For control electrolyte, the peak at 532 eV is assigned to CO_2-like oxygen from lithium alkyl carbonates ($ROCO_2Li$) such as lithium ethylene dicarbonate ($(CH_2OCO_2Li)_2$) (LEDC)[53,54] and/or lithium carbonate (Li_2CO_3) and/or other $ROCO_2Li$ compounds formed by the reduction of EC and EMC. However, for "PES211" electrolyte, the peak at 532 eV was more intense compared to control electrolyte due to the additional O contribution of sulfite species (RSO_3) formed from PES and MMDS as discussed later when the S spectra are considered. This result is in agreement with the higher contribution of the 532 eV components for 2% PES and 1% MMDS electrolytes while the use of TTSPi led to a similar contribution of the 532 eV peak compared to control electrolyte (Figure S3 in the supporting information). For control electrolyte, two additional peaks were observed at ~530.7 and ~528.3 eV and attributed to the formation of lithium alkoxide (ROLi) more likely from EMC[55,56] and lithium oxide (Li_2O),[57,58] respectively. Although the exact formation pathway of Li_2O remains unclear, a reduction of carbonate degradation compounds forming Li_2O[52,59] is more likely than formation of Li_2O from reactions with water.[20] The use of "PES211" electrolyte hindered, however, the formation of ROLi and Li_2O except at 4.7 V most likely due to a beneficial effect of the additives as observed when they were used alone (Figure S3).

The O 1s spectrum of the fresh NMC442 electrode (Figure 6c) showed three components, the first one at 529.5 eV is assigned to O^{2-} anions from the lattice oxygen of the NMC442 while the two other peaks originate from oxygen anions with deficient coordination at the NMC442 surface[50] and/or CO_x-like oxygen from the carbon black[48,49] (referred to as surface oxygen). During formation, the surface oxygen peaks of the fresh electrode were replaced by two components at 531.7 and 533.5 eV in agreement with the formation of carbonaceous species from solvents at the NMC442 surface. These peaks correspond to -CO_2-like oxygen from alkyl carbonates ($ROCO_2Li$) for the 531.7 eV peak and -C-O- bonds from ether derivatives[51,52] and/or $ROCO_2Li$ for the 533.5 eV peak in addition to any remaining contribution of the surface oxygen. At 3.8 V, however, the use of "PES211" led to a higher contribution of the main peak at 531.7 eV compared to control electrolyte. Also, at 3.8 V, the intensity of the 529.5 eV peak from the NMC442 was slightly lowered for control electrolyte compared to

the fresh electrode while it was significantly decreased with the use of "PES211" electrolyte. These results suggest that, similarly to the graphite electrode, "PES211" electrolyte rapidly forms a relatively thick SEI film at the NMC442 surface with a large contribution of oxygen from sulfite species (RSO_3) due to the preferential reaction of both PES and MMDS. This is supported by the lower intensity of the NMC442 peak at 529.5 eV and the higher contribution of the oxygen peak at 531.7 eV for both 2% PES and 1% MMDS electrolytes at 3.8 V while the use of TTSPi led to a similar O 1s spectrum compared to control electrolyte (Figure S4 in the supporting information). At 4.7 V, the intensity of the NMC442 peak at 529.5 eV was further decreased for control electrolyte while it remained almost unchanged for "PES211" electrolyte. Also, the contribution of the -C-O- peak at 533.5 eV continuously increased from 4.4 V to 4.7 V for control electrolyte while with almost no change was found for "PES211". These results indicate that PES 211 forms a relatively stable and passivating SEI film at the NMC442 surface compared to control electrolyte from a thickness perspective anyway (peak at 529.5 eV). This conclusion was confirmed when the cells were discharged to 2.8 V after formation at 4.4 and 4.7 V. Indeed, when PES 211 was used, almost no change in the O 1s spectra of the NMC442 electrode was observed. For control electrolyte, however, the intensity of the NMC442 peak at 529.5 eV significantly increased after discharge after a charge at 4.7 V indicating a partial recovering of the initial SEI film, suggesting instability of the control SEI at high potential. It is therefore concluded that during formation, the use of "PES211" rapidly creates a more stable and passivating SEI film at the NMC442 surface compared to control electrolyte.

Figure 7a shows the sulfur 2p XPS core spectra of graphite and NMC442 electrodes as taken from NMC442/graphite pouch cells with PES 211 electrolyte during formation at 3.8 V and 4.7 V during charge. At 3.8 V, the graphite electrode showed two S 2p components at about 169 and 167 eV while the NMC442 electrode showed one component at about 168.6 eV. For both graphite and NMC442 electrodes, the component centered around 169 eV is assigned to organic sulfite species (RSO_3) such as RSO_3Li and/or $ROSO_2Li$[60] while for the graphite electrodes, the component at ~167 eV can originate from inorganic Li_2SO_3.[60] The S 2p components correspond to the overlap contribution of sulfite species formed from PES and MMDS at 3.8 V (Figure S5 in the supporting information) due to their preferential reactions (Figure 2). At 4.7 V, the intensity of the S 2p components significantly decreased for both electrodes due to the partial covering
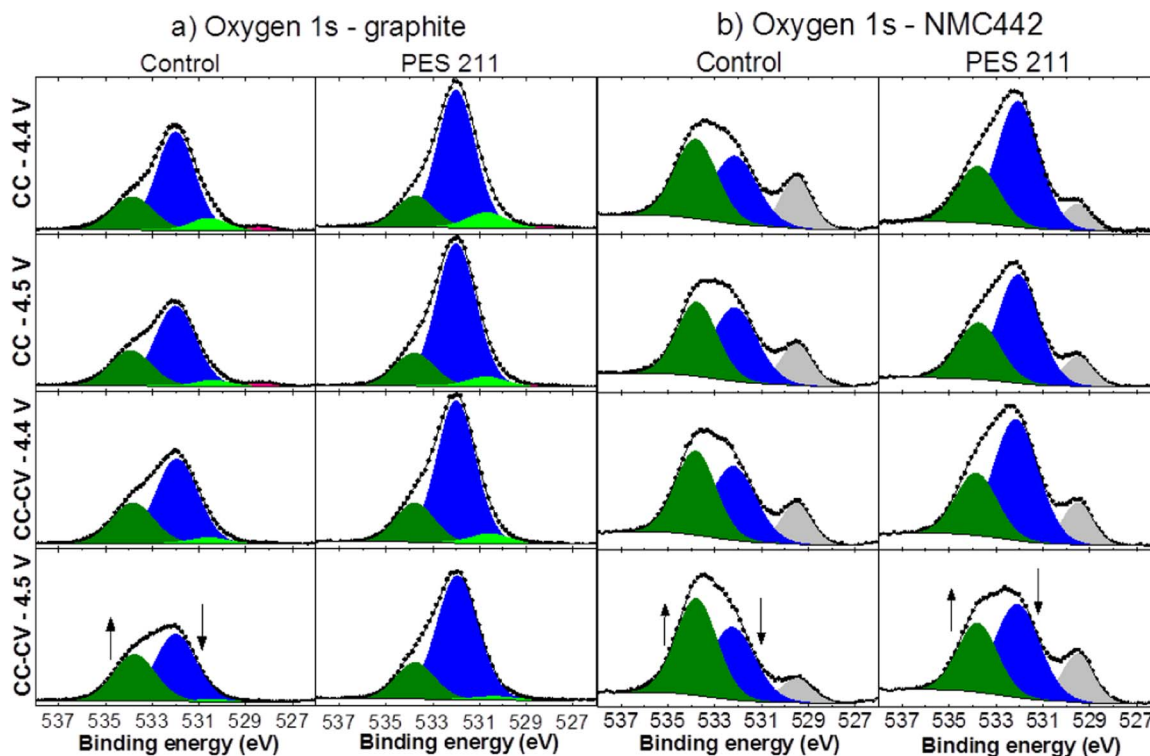
Figure 8. Oxygen 1s XPS core spectra of graphite (a) and NMC442 (b) electrodes for control and "PES211" electrolytes as taken from NMC442/graphite pouch cells after the 25 cycles of CC and charge-hold-discharge (CC-CV) cycling (see Figure 5) at 4.4 and 4.5 V. The cells were stopped at 2.8 V before the XPS spectra were measured.

of the initially formed sulfite species by other SEI compounds generated at high potential. Also, at 4.7 V, two new S 2p peaks appeared at the NMC442 surface at about 166 and 164.2 eV and could be assigned to inorganic Li_2SO_3[60] and $RSSO_3$ (S-like) such as $Li_2S_2O_3$[61] and/or -S- species,[60] respectively. These new sulfur compounds are likely generated by further reaction of relatively unstable sulfite species formed from MMDS as the same phenomenon was observed for 1% MMDS electrolyte and not with the use of PES (Figure S5).

Figure 7b shows the silicon 2p XPS core spectra of the graphite electrodes as taken from NMC442/graphite pouch cells with "PES211" electrolyte during charge at 3.8 V, 4.4 V, 4.5 V and 4.7 V during charge. At 3.8 V, the Si 2p peak observed at about 101.6 eV can be assigned to an organic Si-group such as the initial silyl group from the TTSPi additive. As the full consumption of TTSPi was found by GC-MS before formation and as no electrochemical reaction of TTSPi was observed (Figure 2), it is therefore proposed that TTSPi is either chemically adsorbed and/or grafted at the graphite surface before formation. When further formed to 4.7 V, the intensity of the Si 2p peak significantly decreased in agreement with a preferential reaction of TTSPi at the graphite surface or its covering by other species migrating from the positive electrode at higher potential. This result is supported by a similar evolution of the Si 2p peak at the graphite surface for 1% TTSPi electrolyte (Figure S5 in the supporting information). Note that no Si 2p component was observed at the NMC442 electrodes at any state of charge.

Figures 7c and 7d show the fluorine 1s and phosphorus 2p XPS core spectra of graphite electrodes for control and PES 211 electrolytes as taken from NMC442/graphite pouch cells during formation at 3.8 V, 4.4 V, 4.5 V and 4.7 V during charge. The F 1s spectra showed two peaks at about 687.1 eV and 685 eV attributed to Li_xPF_y[62] and/or $Li_xPO_yF_z$[63] and LiF,[52,64] respectively. The P 2p spectra showed three components at 137.4, 134.8 and 133.5 eV assigned to Li_xPF_y,[62] $Li_xPO_yF_z$[50,64] and phosphates (P_xO_y),[50,64] respectively. Between 3.8 V and 4.5 V, the F 1s and P 2p spectra showed that "PES211" electrolyte

led to a different reactivity of the LiPF$_6$ salt compared to control electrolyte. For instance, higher relative amounts of Li_xPF_y, $Li_xPO_yF_z$ and P_xO_y were found with "PES211" electrolyte. Lower relative amounts of LiF were also observed with "PES211" electrolyte more likely due to the use of PES and MMDS (Figure S6 in the supporting information). Interestingly, at 4.7 V, control electrolyte showed a strong increase in the relative amounts of LiF, $Li_xPO_yF_z$ and P_xO_y and a large decrease of the relative amount of Li_xPF_y while the use of "PES211" electrolyte almost suppressed these phenomena. These results mean that "PES211" electrolyte hinders the degradation of the LiPF$_6$ salt at the positive electrode, reducing the number of species that migrate to the negative electrode, due to the formation of passivating SEI films.

Constant current and charge-hold-discharge (CC-CV) cycling.—Figure 8 shows the oxygen 1s XPS core spectra of graphite (a) and NMC442 (b) electrodes for control and "PES211" electrolytes as taken from NMC442/graphite pouch cells after the 25 cycles of CC and charge-hold-discharge (CC-CV) cycling at 4.4 and 4.5 V. These spectra were taken after discharge to 2.8 V. Figure 8 shows that the chemical nature of the oxygen-containing compounds at both graphite and NMC442 surfaces changes with the upper cutoff potential and the cycling conditions. The ratio of oxygen in a -C-O- environment at 533.8–533.5 eV to a -CO$_2$ environment at 532–531.7 eV increased from 4.4 V to 4.5 V as well as between the CC and charge-hold-discharge (CC-CV) cycling. Finally, the CC-CV cycling at 4.5 V led to the higher -C-O- / -CO$_2$ ratio. These results suggest that further parasitic reactions take place between 4.4 and 4.5 V and/or during long term exposure at 4.4 and 4.5 V. The increase of the relative amount of -C-O- containing compounds could be explained by further reaction of carbonate degradation species such as ROCO$_2$Li and/or by direct degradation of the solvent at the positive electrode through a new reaction pathway at the higher potential. When "PES211" was used, however, the increase of the -C-O- / -CO$_2$ ratio was lowered except during the charge-hold-discharge
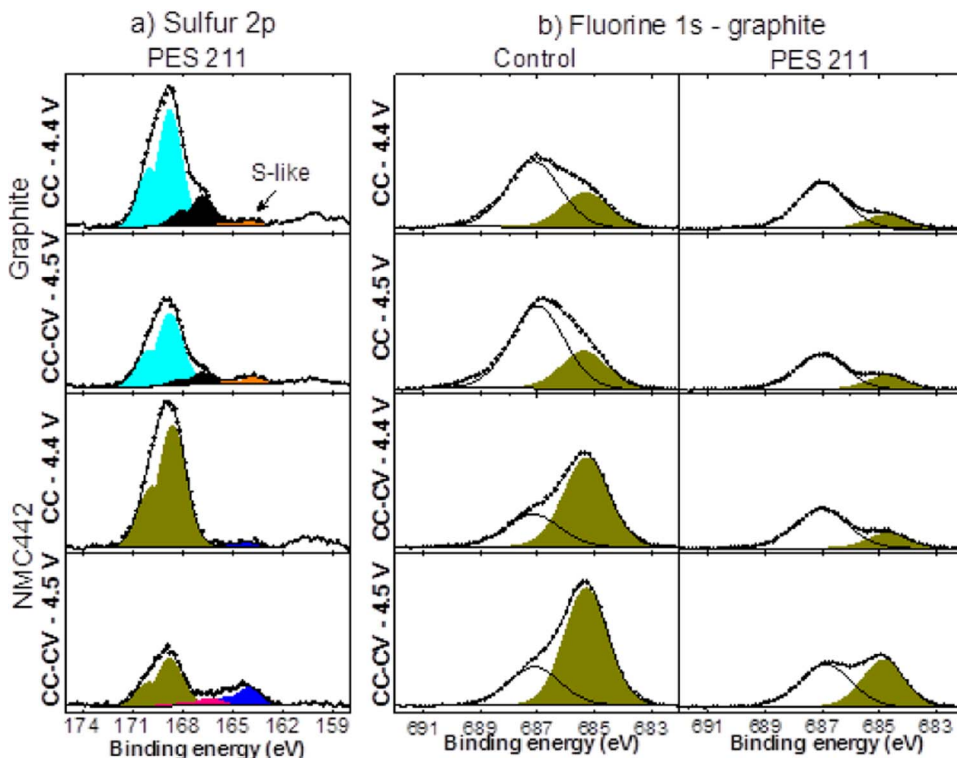
Figure 9. Sulfur 2p (a) XPS core spectra of graphite and NMC442 electrodes for "PES211" electrolyte after the 25 cycles of CC cycling at 4.4 V and the 25 cycles of charge-hold-discharge (CC-CV) cycling at 4.5 V. The cells were discharged to 2.8 V before XPS spectra were taken. Fluorine 1s (b) XPS core spectra of graphite electrodes for control and "PES211" electrolyte taken from the same NMC442/graphite pouch cells as in Figure 9a.

(CC-CV) cycling at 4.5 V. Therefore, the use of "PES211" electrolyte can help stabilize the graphite and NMC442 SEI films compared to control electrolyte in agreement with the improved capacity retention (Figure 2 and 5) and lower gas production (Figure 4).

Figure 9a shows the sulfur 2p XPS core spectra of graphite and NMC442 electrodes as taken from NMC442/graphite pouch cells with "PES211" electrolyte after the 25 cycles of CC cycling at 4.4 V and after the 25 cycles of charge-hold-discharge (CC-CV) cycling at 4.5 V. The cells were discharged to 2.8 V before the XPS spectra were measured. At the NMC442 surface, the two weak peaks at about 166 eV (Li_2SO_3) and 164.2 eV (S-like) were assigned to further reaction of sulfite species as previously observed during formation (Figure 7a). At the graphite surface, a new S 2p component was observed at ∼163.9 eV after cycling and is also assigned to further reaction of sulfite species. Interestingly, the relative amounts of these new sulfur compounds increased for the charge-hold-discharge (CC-CV) cycling at 4.5 V compared to the CC cycling at 4.4 V. This result indicates a relatively poor stability of the sulfite species and the resulting SEI films when exposed for a long time at 4.5 V. This is supported by a lower relative amount of organic sulfite species (peak at about 169 eV) during the charge-hold-discharge (CC-CV) cycling at 4.5 V due to both the further reaction of the sulfite species and a partial covering by other SEI compounds.

Figure 9b shows the fluorine 1s XPS core spectra of graphite electrodes for control and "PES211" electrolytes as taken from NMC442/graphite pouch cells after the CC and charge-hold-discharge (CC-CV) cycling at 4.4 and 4.5 V. The cells were discharged to 2.8 V before XPS spectra were acquired. As observed during formation (Figure 7c), the use of "PES211" electrolyte led to significantly lower relative amounts of LiF at the graphite surface especially when the charge-hold-discharge (CC-CV) cycling was used. This result suggests that "PES211" electrolyte continues to hinder the degradation of the $LiPF_6$ salt due to the formation of passivating SEI films.

Conclusions

The effects of a ternary additive system 2% PES + 1% MMDS + 1% TTSPi ("PES211") in NMC442/graphite pouch cells balanced for 4.7 V was thoroughly investigated. The use of "PES211" electrolyte significantly improved the capacity retention, impedance and gas formation of NMC442/graphite pouch cells cycled at constant current (CC) up to 4.4 or 4.5 V compared to control electrolyte. When cycled using a charge-hold-discharge (CC-CV, with a 20 h hold at top of charge) protocol, however, the NMC442/graphite pouch cells filled with "PES211" electrolyte displayed capacity loss, impedance increase and gas formation, especially at 4.5 V, which indicates that extensive electrolyte degradation occurs as soon as the cells are exposed for long periods of time at potentials above 4.4 V.

XPS analysis of the SEI films showed that during formation, "PES211" electrolyte rapidly creates more stable and passivating SEI films at both the graphite and NMC442 surfaces compared to control electrolyte apparently due to the preferential reaction of PES and MMDS. It was found that TTSPi also reacts at the graphite surface through a chemical reaction even before the cells are charged for the first time. The use of "PES211" also modifies the reactivity of the $LiPF_6$ salt at the NMC surface and hinders its degradation during formation at high voltage (4.7 V) and after long time exposure at high potential (CC-CV). Additionally, "PES211" almost eliminated changes to the chemical nature of the oxygen-containing compounds observed at both graphite and NMC442 surfaces (i.e. the increase of the -C-O- / -CO_2 ratio) except for the case of long time exposure (CC-CV) at 4.5 V. These results indicated the passivating effect of the SEI films formed with "PES211" electrolyte at both the graphite and NMC442 surfaces which led to better capacity retention and lower gas production. However, a relatively poor stability of the sulfite species and the resulting SEI films was observed with "PES211" electrolyte when exposed for long times at 4.5 V.

References

1. W. Huang, L. Xing, Y. Wang, M. Xu, W. Li, F. Xie, and S. Xia, *J. Power Sources*, **267**, 560 (2014).
2. L. Xia, Y. Xia, and Z. Liu, *Electrochimica Acta*, **151**, 429 (2015).
3. S. S. Zhang, *J. Power Sources*, **162**, 1379 (2006).
4. K. Xu, *Chem. Rev.*, **104**, 4303 (2004).
5. E. Peled, *J. Electrochem. Soc.*, **126**, 2047 (1979).
6. http://www.google.com/patents/US5626981.
7. M. Contestabile, M. Morselli, R. Paraventi, and R. J. Neat, *J. Power Sources*, **119–121**, 943 (2003).
8. M. Holzapfel, C. Jost, A. Prodi-Schwab, F. Krumeich, A. Würsig, H. Buqa, and P. Novák, *Carbon*, **43**, 1488 (2005).
9. T. Sasaki, T. Abe, Y. Iriyama, M. Inaba, and Z. Ogumi, *J. Electrochem. Soc.*, **152**, A2046 (2005).
10. E.-G. Shim, T.-H. Nam, J.-G. Kim, H.-S. Kim, and S.-I. Moon, *J. Power Sources*, **172**, 901 (2007).
11. L. Chen, K. Wang, X. Xie, and J. Xie, *J. Power Sources*, **174**, 538 (2007).
12. N. N. Sinha, A. J. Smith, J. C. Burns, G. Jain, K. W. Eberman, E. Scott, J. P. Gardner, and J. R. Dahn, *J. Electrochem. Soc.*, **158**, A1194 (2011).
13. J. C. Burns, G. Jain, A. J. Smith, K. W. Eberman, E. Scott, J. P. Gardner, and J. R. Dahn, *J. Electrochem. Soc.*, **158**, A255 (2011).
14. J. Jeon, S. Yoon, T. Park, J.-J. Cho, S. Kang, Y.-K. Han, and H. Lee, *J. Mater. Chem.*, **22**, 21003 (2012).
15. H. M. Jung, S.-H. Park, J. Jeon, Y. Choi, S. Yoon, J.-J. Cho, S. Oh, S. Kang, Y.-K. Han, and H. Lee, *J. Mater. Chem. A*, **1**, 11975 (2013).
16. J. Xia, N. N. Sinha, L. P. Chen, G. Y. Kim, D. J. Xiong, and J. R. Dahn, *J. Electrochem. Soc.*, **161**, A84 (2014).
17. J. Xia, N. N. Sinha, L. P. Chen, and J. R. Dahn, *J. Electrochem. Soc.*, **161**, A264 (2014).
18. J. Xia, J. E. Harlow, R. Petibon, J. C. Burns, L. P. Chen, and J. R. Dahn, *J. Electrochem. Soc.*, **161**, A547 (2014).
19. P. Janssen, R. Schmitz, R. Müller, P. Isken, A. Lex-Balducci, C. Schreiner, M. Winter, I. Cekić-Laskovic, and R. Schmitz, *Electrochimica Acta*, **125**, 101 (2014).
20. L. Madec, J. Xia, R. Petibon, K. J. Nelson, J.-P. Sun, I. G. Hill, and J. R. Dahn, *J. Phys. Chem. C* (2014) .
21. B. Li, M. Xu, T. Li, W. Li, and S. Hu, *Electrochem. Commun.*, **17**, 92 (2012).
22. B. Li, M. Xu, B. Li, Y. Liu, L. Yang, W. Li, and S. Hu, *Electrochimica Acta*, **105**, 1 (2013).
23. B. Li, Y. Wang, W. Tu, Z. Wang, M. Xu, L. Xing, and W. Li, *Electrochimica Acta*, **147**, 636 (2014).
24. B. Li, Y. Wang, H. Rong, Y. Wang, J. Liu, L. Xing, M. Xu, and W. Li, *J. Mater. Chem. A*, **1**, 12954 (2013).
25. J. Xia, L. Ma, C. P. Aiken, K. J. Nelson, L. P. Chen, and J. R. Dahn, *J. Electrochem. Soc.*, **161**, A1634 (2014).
26. K. J. Nelson, J. Xia, and J. R. Dahn, *J. Electrochem. Soc.*, **161**, A1884 (2014).
27. L. Madec, R. Petibon, J. Xia, J.-P. Sun, I. G. Hill, and J. R. Dahn, *J. Electrochem. Soc.*, **162**, A2635 (2015).
28. X. Zuo, C. Fan, X. Xiao, J. Liu, and J. Nan, *J. Power Sources*, **219**, 94 (2012).
29. X. Zuo, C. Fan, X. Xiao, J. Liu, and J. Nan, *ECS Electrochem. Lett.*, **1**, A50 (2012).
30. X. Zuo, J. Wu, C. Fan, K. Lai, J. Liu, and J. Nan, *Electrochimica Acta*, **130**, 778 (2014).
31. T. Huang, M. Wu, W. Wang, Y. Pan, and G. Fang, *J. Power Sources*, **262**, 303 (2014).
32. F. Bian, Z. Zhang, and Y. Yang, *J. Energy Chem.*, **23**, 383 (2014).
33. V. Bhat, G. Cheng, S. Kaye, B. Li, R. Olugbile, and J. H. Yang, (2012) http://www.google.com/patents/US20120315536.
34. N. N. Sinha, J. C. Burns, and J. R. Dahn, *J. Electrochem. Soc.*, **161**, A1084 (2014).
35. S. Mai, M. Xu, X. Liao, J. Hu, H. Lin, L. Xing, Y. Liao, X. Li, and W. Li, *Electrochimica Acta*, **147**, 565 (2014).
36. Y.-M. Song, J.-G. Han, S. Park, K. T. Lee, and N.-S. Choi, *J. Mater. Chem. A*, **2**, 9506 (2014).
37. T. Yim, S.-G. Woo, S. H. Lim, W. Cho, J. H. Song, Y.-K. Han, and Y.-J. Kim, *J. Mater. Chem. A*, **3**, 6157 (2015).
38. L. Ma, J. Xia, and J. R. Dahn, *J. Electrochem. Soc.*, **161**, A2250 (2014).
39. L. Ma, J. Xia, and J. R. Dahn, *J. Electrochem. Soc.*, **162**, A1170 (2015).
40. K. J. Nelson, G. L. d'Eon, A. T. B. Wright, L. Ma, J. Xia, and J. R. Dahn, *J. Electrochem. Soc.*, **162**, A1046 (2015).
41. K. J. Nelson, G. L. d'Eon, A. T. B. Wright, L. Ma, J. Xia, and J. R. Dahn, *J. Electrochem. Soc.*, **162**, A1046 (2015).
42. C. P. Aiken, J. Xia, D. Y. Wang, D. A. Stevens, S. Trussler, and J. R. Dahn, *J. Electrochem. Soc.*, **161**, A1548 (2014).
43. D. A. Shirley, *Phys. Rev. B*, **5**, 4709 (1972).
44. G. V. Zhuang, K. Xu, H. Yang, T. R. Jow, and P. N. Ross, *J. Phys. Chem. B*, **109**, 17567 (2005).
45. K. Xu, Y. Lam, S. S. Zhang, T. R. Jow, and T. B. Curtis, *J. Phys. Chem. C*, **111**, 7411 (2007).
46. R. Petibon, L. Rotermund, K. J. Nelson, A. S. Gozdz, J. Xia, and J. R. Dahn, *J. Electrochem. Soc.*, **161**, A1167 (2014).
47. R. Petibon, J. Xia, J. C. Burns, and J. R. Dahn, *J. Electrochem. Soc.*, **161**, A1618 (2014).
48. D. Pantea, H. Darmstadt, S. Kaliaguine, L. Sümmchen, and C. Roy, *Carbon*, **39**, 1147 (2001).
49. D. Pantea, H. Darmstadt, S. Kaliaguine, and C. Roy, *Appl. Surf. Sci.*, **217**, 181 (2003).
50. L. E. Ouatani, R. Dedryvère, C. Siret, P. Biensan, S. Reynaud, P. Iratçabal, and D. Gonbeau, *J. Electrochem. Soc.*, **156**, A103 (2009).
51. R. Dedryvère, L. Gireaud, S. Grugeon, S. Laruelle, J.-M. Tarascon, and D. Gonbeau, *J. Phys. Chem. B*, **109**, 15868 (2005).
52. S. Malmgren, K. Ciosek, M. Hahlin, T. Gustafsson, M. Gorgoi, H. Rensmo, and K. Edström, *Electrochimica Acta*, **97**, 23 (2013).
53. D. Aurbach, M. L. Daroux, P. W. Faguy, and E. Yeager, *J. Electrochem. Soc.*, **134**, 1611 (1987).
54. M. Nie, D. Chalasani, D. P. Abraham, Y. Chen, A. Bose, and B. L. Lucht, *J. Phys. Chem. C*, **117**, 1257 (2013).
55. M. Onuki, S. Kinoshita, Y. Sakata, M. Yanagidate, Y. Otake, M. Ue, and M. Deguchi, *J. Electrochem. Soc.*, **155**, A794 (2008).
56. R. Petibon, L. M. Rotermund, and J. R. Dahn, *J. Power Sources*, **287**, 184 (2015).
57. I. Ismail, A. Noda, A. Nishimoto, and M. Watanabe, *Electrochimica Acta*, **46**, 1595 (2001).
58. L. J. Rendek, G. S. Chottiner, and D. A. Scherson, *J. Electrochem. Soc.*, **149**, E408 (2002).
59. S.-P. Kim, A. C. T. van Duin, and V. B. Shenoy, *J. Power Sources*, **196**, 8590 (2011).
60. H. Ota, H. Akai, H. Namita, S. Yamaguchi, and M. Nomura, *J. Power Sources*, **119–121**, 567 (2003).
61. S. Xiong, K. Xie, Y. Diao, and X. Hong, *J. Power Sources*, **246**, 840 (2014).
62. K. Edström, T. Gustafsson, and J. O. Thomas, *Electrochimica Acta*, **50**, 397 (2004).
63. B. Ravdel, K. M. Abraham, R. Gitzendanner, J. DiCarlo, B. Lucht, and C. Campion, *J. Power Sources*, **119–121**, 805 (2003).
64. H. Bouayad, Z. Wang, N. Dupré, R. Dedryvère, D. Foix, S. Franger, J.-F. Martin, L. Boutafa, D. Patoux, D. Gonbeau, and D. Guyomard, *J. Phys. Chem. C*, **118**, 4634 (2014).